Artificial intelligence for fast and accurate 3D tooth segmentation on CBCT

Pierre Lahoud, DDS, Mostafa EzEldeen, DDS, MScD, Thomas Beznik, Holger Willems, André Leite, DDS, MSc, PhD, Adrian Van Gerven, Reinhilde Jacobs, DDS, MSc, PhD

PII: S0099-2399(21)00004-2

DOI: https://doi.org/10.1016/j.joen.2020.12.020

Reference: JOEN 4769

To appear in: *Journal of Endodontics*

Received Date: 6 August 2020

Revised Date: 25 December 2020

Accepted Date: 30 December 2020

Please cite this article as: Lahoud P, EzEldeen M, Beznik T, Willems H, Leite A, Van Gerven A, Jacobs R, Artificial intelligence for fast and accurate 3D tooth segmentation on CBCT, *Journal of Endodontics* (2021), doi: https://doi.org/10.1016/j.joen.2020.12.020.

Artificial intelligence for fast and accurate 3D tooth segmentation on CBCT

Authors: Pierre Lahoud, DDS[1] ; Mostafa EzEldeen, DDS, MScD[1,2] ; Thomas Beznik[3] ; Holger Willems[3] ; André Leite, DDS, MSc, PhD[1,4] ; Adrian Van Gerven[3], Reinhilde Jacobs, DDS, MSc, PhD[1,5]

[1]OMFS IMPATH Research Group, Department of Imaging & Pathology, Faculty of Medicine, University of Leuven and Oral & Maxillofacial Surgery, University Hospitals Leuven, Leuven, Belgium

[2]Department of Oral Health Sciences, KU Leuven and Paediatric Dentistry and Special Dental Care, University Hospitals Leuven, Leuven, Belgium

[3]Relu, R&D, 3000 Leuven, Belgium.

[4]Department of Dentistry, Faculty of Health Sciences, University of Brasília, Brasília, Brazil

[5]Oral facial diagnostics and surgery, Department of Dental Medicine, Karolinska Institute, Stockholm, Sweden

The authors deny any conflicts of interest.

Corresponding author:

Mostafa EzEldeen DDS, MScD

OMFS IMPATH Research Group, Faculty of Medicine, Department of Imaging and Pathology, KU Leuven and Oral and Maxillofacial Surgery, University Hospitals Leuven, Kapucijnenvoer 33, 3000 Leuven, Belgium.

E-mail address: mostafa.ezeldeen@kuleuven.be

Artificial intelligence for fast and accurate 3D tooth segmentation on CBCT

ABSTRACT

Introduction: Tooth segmentation on CBCT is a labour-intensive task, considering limited contrast resolution and potential disturbance by various artefacts. Fully automated tooth segmentation cannot be achieved by merely relying on CBCT intensity variations. This study aimed to develop and validate an artificial intelligence (AI)-driven tool for automated tooth segmentation on CBCT.

Methods: Total of 433 DICOM images of single and double rooted teeth randomly selected from 314 anonymized CBCT scans were imported and manually segmented. An AI-driven tooth segmentation algorithm based on a feature pyramid network (FPN) was developed to automatically detect and segment teeth replacing manual user contour placement. The AI-driven tool was evaluated based on volume comparison, intersection over union (*IoU*), Dice score coefficient (DSC), morphologic surface deviation and total segmentation time.

Results: Overall, AI-driven and clinical reference segmentations resulted in very similar segmentation volumes. The mean *IoU* for full tooth segmentation was 0.87 (±0.03) and 0.88 (±0.03) for semi-automated (SA) (clinical reference) vs fully automated AI-driven (F-AI) and refined AI-driven (R-AI) respectively. R-AI and F-AI showed an average median surface deviation from SA of 9.96 µm (±59.33) and 7.85 µm (±69.55) respectively. SA segmentations of single and double rooted teeth had a mean total time of 6.6 mins (±76.15s), F-AI of 0.5 mins (±8.64s) (12 times faster) and R-AI of 1.2 mins (±33.02s) (6 times faster).

Conclusion: This study demonstrated a unique fast and accurate approach for AI-driven automated tooth segmentation on CBCT. Results may open doors for AI-driven applications in surgical and treatment planning in oral healthcare.

Introduction

Dentistry excels in the delivery of personalized healthcare, traditionally through fabrication of dental fillings, crowns and prostheses. The last two decades have seen an exponential rise in the field of three-dimensional (3D) image analysis and printing techniques leading to multiple digital dentistry (DD) applications. Amongst the most frequent applications are 3D-guided implant surgery (1), guided-endodontics and apical surgeries (2, 3) CBCT-based planning and fabrication of donor teeth replicas and surgical guides for successful tooth autotransplantation (TAT) (4), digital orthodontic applications (5) and virtual orthognathic surgery planning (6).

DD relies primarily on acquisition and segmentation of 3D imaging modalities. The current trend of image acquisition in this field relies primarily on cone beam computed tomography (CBCT), which offers highly accurate volumetric data on jaw bones and teeth with relatively low radiation doses and cost, (7-9).

Image segmentation is a process of dividing an image into different meaningful regions and is utilized in structural identification and quantitative assessment of dental structures for various imaging modalities (10, 11). Tooth segmentation is vital for accurate diagnosis, treatment planning and direct surgical assistance for a wide variety of DD applications as abovementioned.

Nevertheless, teeth segmentation on CBCT remains a labour-intensive and challenging task, primarily related to the lack of hounsfield units (HUs) and the limited differential contrast between cementum, dentin and bone with only 200 µm-wide periodontal ligament space. Meanwhile these images also suffer from artefacts in the jaw bone area, making fully automated tooth segmentation by merely relying on intensity variation of (CB)CT images unreliable (5).

Convolutional neural networks (CNN/ConvNet) are a special type of deep learning (DL) algorithms made of multilayer neural networks, specifically aimed at the recognition of visual

patterns from pixelized images with minimal pre-processing (12). Several CNNs have been described with different architectures depending on the application (13, 14). CNNs sparked tremendous interest over the past few years, and have become relevant tools for image processing and segmentation (11, 15), such as the use of U-Net and V-Net for automated level set-based tooth segmentation (16, 17). The architecture of a CNN is analogous to that of the connectivity pattern of neurons in the human brain; mainly inspired by the organization of the visual cortex. A CNN "learns" intrinsic statistical patterns in data to eventually cast predictions on unseen data (18). Implementation of a CNN in a tooth segmentation tool could help improving the results, given that the algorithm could be taught how to behave for challenging – yet highly common – cases, including complicated root anatomy, heavy scattering, immature teeth and metal artefacts. Such tool could bridge the gap between accuracy and time consumption for tooth segmentation, and potentially simplify digital dentistry applications and surgical planning to a broader audience of practitioners.

Frequently used tooth segmentation software mainly relies on thresholding, template-based fitting methods (TbFM) and level set methods to segment individual tooth from dental CBCT images.

However, thresholding may not work if underlying shading distorts the image and may have difficulties finding the threshold minimum (19), especially with CBCT grey values. TbFM lacked robustness with multi-rooted teeth and complex anatomy (16), while the level set method needs to perform numerous mathematical operations, yielding relatively slow results (20) and may be problematic in regards to partial volume effects, especially when the intensity variation in the background is higher than in the foreground (21). Also, the use of such automated methods could struggle with images of low quality, metal artefacts and immature tooth segmentation.

The overall aim of this study was to develop and validate a clinically operational AI-driven tooth segmentation tool capable of minimizing manual interventions and yielding fast, accurate and consistent results essential for clinical use.

Materials and Methods

Data Acquisition and Training Database

CBCT scans were randomly collected from two previous study databases, described in supplemental S1. All teeth were segmented manually by experts in the field of dentomaxillofacial radiology using a dedicated tool developed in MeVisLab (MeVis Research, Bremen, Germany) and validated for accurate tooth/root and canal space segmentation as previously described (10) with an integrated time monitoring module. Briefly, the imaging analysis tool applies a semi-interactive livewire boundary extraction (22) to create a set of orthogonal contours, followed by a variational interpolation algorithm that reconstructs the surface of an object with energy-minimizing, smoothening and implicit functions (23). Segmentations resulted in a total of 433 DICOM (digital imaging and communications in medicine) images of teeth randomly selected from the CBCT scans – including upper and lower incisors, canines and premolars – accounting for 2924 slice images of teeth sampled in axial, sagittal or coronal direction and an associated binary mask identifying the region of the image belonging to the tooth. Each binary mask was generated based on a contour segmentation object file (CSO file) of the tooth, that were annotated on the 2D slices. Contours were filled and exported as portable network graphics (PNG) images, while the corresponding slice was extracted from the 3D DICOM image and exported to a grayscale PNG image. These 2D image pairs were then divided into three datasets: training (2095 samples, 71.6%), optimization (501 samples, 17.2%) and validation set (328 samples, 11.2%). Datasets included single and double

rooted teeth (with mature and immature cases), various artefacts, fillings, metal posts, low resolution images, various voxel sizes, heavy and low scattering as well as other segmentation-challenging cases.

Machine Learning

Dataset pre-processing and augmentation

Data augmentation techniques were used on the training set in order to increase the generalization and robustness of the model, as detailed in supplemental S2.1.

Network Architecture of the ConvNet

The architecture used was a Feature Pyramid Network (FPN) (24). Network architecture is demonstrated in figure 1. Detailed description is provided in supplemental S2.2.

AI driven tooth segmentation

An AI-driven tooth segmentation algorithm trained with the above described dataset was developed for automated detection and segmentation of tooth structure replacing manual user contour placement implemented in the previously validated tooth segmentation method (10). Moreover, the possibility of user interaction was preserved with the ability to modify, add, or delete the AI suggested contours (figure 2).

Validation Dataset

Forty-six randomly selected cases were chosen for the validation of the tool. These cases accounted for 10% of the whole database (433 DICOMs) and were unseen by the algorithm during the training phase. The validation set consisted of 19 incisors, 17 canines and 17 premolars, equally proportional to the full database tooth-type distribution.

All 46 cases were segmented using three segmentation protocols: (1) semi-automated segmentation (SA) – performed manually by experts in the field of oral radiology and medical

imaging and serving as the clinical reference – which relied on the use of livewire contour based segmentation as described earlier (10) and without AI assistance, (2) fully automated AI-driven segmentation (F-AI) – where no user interaction was performed following the AI-computation and contour placement; and (3) refined AI-driven segmentation (R-AI) – where expert users refine what was judged under- or over-estimated following computation suggested by the AI-algorithm.

Assessment and Validation of the tool

Voxel-based performance metrics

Binarized segmentation results were used for volume calculation and subsequent assessment. The binary images were fed to an Intersection-Over-Union (*IoU*) algorithm to test for the accuracy of overlap (25). The module plotted F-AI and R-AI groups against SA in order to evaluate the performance of the AI-tool. An *IoU* score lower than 0.5 is considered as failure (26). Further, the Dice similarity coefficient (*DSC*) was calculated for each tooth/protocol (F-AI & R-AI) versus the reference image (SA).

IoU is employed as a loss function in foreground and background classification tasks of object in an image (25). Detailed calculation steps are available in supplemental S3.

3D Reconstruction and Morphologic Surface Analysis

After segmentation, the 3D triangle-based surface of the tooth was reconstructed as a Standard Tessellation Language file (STL). All STL files were then imported in the 3-matic software (Materialise NV, Leuven, Belgium) to perform a signed morphologic surface comparison between the 3D model for each tooth/protocol (F-AI & R-AI) versus the 3D model from the reference image (SA), allowing for positive and negative differentiation with regard to the

reference image (figure 2-L/M). A cutoff value for accuracy was set at 200µm median surface deviation from the reference image (27, 28).

Statistical Analysis

Results from the metrics calculated during and after segmentation were evaluated in regard to three distinct groups: (1) Full dataset analysis, (2) mature and immature tooth analysis, and (3) tooth-types dependent analysis (for incisors, canines and premolars separately).

Statistical analysis was performed using GraphPad Prism for MacOS, version 9.0. (GraphPad Software, La Jolla California, USA). Volume variation between the three groups as well as between the different tooth types and condition (mature and immature) was reported in a descriptive fashion. The systematic volume deviation between F-AI, R-AI and SA segmentations was evaluated using the method of Bland and Altman (29) in MedCalc for Windows, version 15.0 (MedCalc Software, Ostend, Belgium). Detailed timing was recorded and compared between the three groups using repeated measuresAnalysis of Variance (ANOVA) method with Tukey's correction. To examine if AI segmentations were not inferior to the SA segmentations (dentist-operated) two metrics were evaluated as follows: 1- the *IoU* scores for F-AI and R-AI were tested using a one-sample t-test (an *IoU* score lower than 0.5 is considered as failure), 2- average surface deviation using a one-sample t-test against a cut-off value of 200 µm.

A two-way ANOVA test with Tukey's correction was used to evaluate the effect of tooth type (incisors, canines and premolars) and apex maturation on the *IoU* score of F-AI as well as R-AI. All measurements were calculated for the overall tooth as well as for crown and root separately.

Results

Overall, AI-driven and clinical reference segmentations resulted in very similar segmentation volumes (figure 3A). The mean segmentation volume for the SA (clinical reference) was 544 mm^3 (±121), while this was 536 mm^3 (±121) and 538 mm^3 (±123) for the F-AI and the R-AI methods, respectively. The deviation in segmented volumes between F-AI and R-AI versus SA (clinical reference) was evaluated using the Bland-Altman method showing a systematic decrease in segmentation volume 1.7% for F-AI and 1.3% for R-AI (figure 3B-C).

The mean *IoU* for full tooth segmentation was 0.87 (±0.03) and 0.88 (±0.03) for SA vs F-AI and R-AI respectively. Both F-AI and R-AI performed as good as the human operator *($p<0.0001$)*, without any failure cases (*IoU* score below 0.5) (figure 4D). The mean DSC 0.93 was (±0.02) and 0.94 (±0.02) for SA vs F-AI and R-AI respectively.

There was a significant effect on the *IoU* score at the $p<0.05$ for tooth types included in this study (incisors, canines and premolars) [$F(2, 88) = 21.9$, $p<0.0001$]. Post hoc comparisons using the Tukey test indicated that the mean *IoU* score for incisors (full tooth and crown segmentations) was significantly different than canines and premolars in both the F-AI and R-AI groups. Detailed *IoU* results are shown in table 1. While, there was no significant effect on the *IoU* score at the $p<0.05$ for the tooth apex maturation (mature vs. immature) [$F(1, 89) = 0.1145$, $p=0.73$].

A morphologic surface comparison between SA versus F-AI and R-AI showed an average median surface deviation of 7.85 µm (±69.55) and 9.96 µm (±59.33) (figure 3E). Both F-AI and R-AI performed as good as the human operator *($p<0.0001$)*, without average surface deviation higher than the cut-off value of 200 µm (figure 3E, F and G).

There was a significant effect on the total time consumed at the $p<0.05$ for the three segmentation methods [$F(2, 144) = 847$, $p<0.0001$]. Post hoc comparisons using the Tukey test

indicated that the SA segmentations time (mean = 6.6 mins ±76.2s) was significantly different from the F-AI (mean = 0.5 mins ±8.6s) and R-AI (mean = 1.2 mins ±33.0s) segmentations. This difference demonstrated a 12.5- and 6.5-fold decrease in the segmentation time for the F-AI and R-AI respectively. The difference in segmentation time between F-AI and R-AI was statistically significant *(p-value <0.05).* The aforementioned total time accounted for region of interest (ROI) selection, rotation, seeds/contour placement and image saving (figure 2). In case of AI-driven segmentations (F-AI / R-AI), the average time needed by the user for ROI selection, rotation and saving was 29.7 seconds (±8.6s), and the average time needed by the algorithm to cast segmentation predictions on slices had a mean of 1.7 seconds (±0.04s). Additional user interactions for R-AI segmentations then took an average of 55 seconds (±2.5s).

Discussion

This study reports on the development and validation of a novel tool for automated tooth segmentation based on AI. The presented data confirms the positive impact of implementing AI technology in the field of radiology in general and segmentation in particular, highlighting the high accuracy and low time-consumption gained from AI integration.

Despite the heterogeneity of the dataset used in terms of age, image quality, voxel size and artefacts, no failure cases ($IoU < 0.5$) were recorded and no cases showed an *IoU* rate below 0.77 – illustrating the wide array of clinical cases to which this tool can be applied. It must be stated that the *IoU* penalizes just a slight shift in overlap quite heavily. Therefore, a good overlap has an $IoU > 0.6$, and an excellent overlap has an *IoU* of > 0.9 (26).

AI integration for tooth segmentation bridges the gap between automated segmentation and challenging cases such as immature teeth, teeth with fillings and metal induced artefacts. Previous studies applying automated segmentation methods using techniques such as the level-

set or template-based fitting method for tooth segmentation (5), showed drawbacks obtaining highly accurate results on such challenging clinical cases, yet highly common in daily clinical practice.

CNNs have been introduced by (30) in the early 1990's. They rely on hidden layers responsible of feature extraction and classification and have showed excellent results in detection and classification tasks (31). In the current study a feature pyramid networks architecture was selected (24), since it is part of the state-of-the-art of semantic segmentation and because it showed from our preliminary results an acceptable inference time of approximately 1.6 seconds. As for the encoder, an efficientnet-b7 was used, as it achieves superior performances on the ImageNet dataset, while using less operations than other encoders such as ResNet (32).

To date, few attempts of bridging AI and tooth segmentation were reported. Cui et al. (5) relied on a 2-stage approach with two 3D networks, requiring specialized software and advanced hardware to run efficiently. The sample size used in the study was relatively small (12 images for training and 8 for validation). Timing and comparison with manual segmentations were not reported, and no cases with artefacts were used. Moreover, DSC reached at most 0.921.

Chen et al. (16) used a multi-task 3D fully convolutional network (V-Net) based on 3D operation to predict tooth region and surface. This approach had a maximum DSC of 0.94 (± 0.01) and similar to the Cui et al.'s relies on a 3D approach, requiring heavy processing.

Lee et al.'s (17) used a 2D U-Net to label slice-by-slice, yet relied on mapping Grey values to HUs, which has been proven to be unreliable on CBCT even after normalization (33).

None of the approaches discussed reported the possibility of manual corrections or user interaction to enhance the AI-driven segmentations. Further, editing a 3D label-map is computationally demanding, as it requires going through the slices and editing on a voxel basis.

Such methods may yield relatively slow results and require GPU to efficiently operate, complicating accurate user-interaction and manual corrections. Therefore, the aforementioned approaches might struggle with complex images, heavy scattering and other compromising radiological artefacts. In contrast to the 2D slice correction and interpolation approach applied in the current study.

This present study tackled these issues by exposing the algorithm to a large dataset with 314 CBCT scans, yielding 2924 fully segmented CSO paths for the study and diverse cases such as root shape variation, heavy scattering, restorations, orthodontic brackets, artefacts and resorptions. The method applied in the current study also allows for smooth user-interaction with the dentist in mind as an end-user. The operator is able to correct what is judged under- or over-estimated in a user-friendly and highly intuitive interface, given that the segmentations rely on CSOs seed points and contours on 2D images, which can easily be adjusted to precise locations, as well as having more seeds/contours added or removed – according to the operator's judgment. To the best of our knowledge, this is the first attempt of AI-driven tooth segmentation based on CSOs and 2D slices, that is combined with a previously validated interpolation algorithm for accurate 3D teeth segmentation (10). This tool can be operated without GPU and therefore on personal computers and could also be implemented as a cloud-based service, serving a wider audience for DD applications.

It is fair to mention that this study has its own limitations. The AI algorithm was not trained to segment molars yet (figure 1). It can therefore segment from second premolar to second premolar in both the maxilla and mandible. The tool can also segment one tooth at a time and require a manual ROI selection and rotation, however both will be automated in the near future. Nevertheless, the results obtained are unique showing the effectiveness of this technique in terms

of fully automated segmentations and provide the best results to date in terms of accuracy and time consumption for AI-driven teeth segmentations. The developed tool has a direct clinical application in guided-endodontics, CBCT-based TAT and orthodontic treatment planning and follow-up. Moreover, in research, the tool will simplify studying the 3D tooth root tissue changes after regenerative endodontic procedures (10, 34, 35), TAT (4) and orthodontic tooth movement. Studying the 3D patterns of tissue deposition or resorption could offer valuable insights into the treatment outcomes and influence clinical decision making.

Conclusion

The present study demonstrated a novel approach for using CNNs for accurate and fast automated 3D tooth segmentation. The aforementioned results may open doors for AI-driven applications in surgical and treatment planning for improving efficiency and accuracy of various procedures in oral surgery, orthodontics, guided-endodontics, tooth autotransplantation.

Author Contributions

P. Lahoud, M. EzEldeen, T. Beznik and R. Jacobs contributed to conception, design, data acquisition, analysis, and interpretation, drafted and critically revised the manuscript; A. Leite, contributed to data acquisition, analysis, and interpretation, critically revised the manuscript; H. Willems and A. Van Gerven, contributed to contributed to conception and design, critically revised the manuscript. All authors gave final approval and agree to be accountable for all aspects of the work.

Acknowledgments

Supported by Research Council of KU Leuven grant number (C24/18/068).

The authors would like to thank Dr. Wim Coucke for statistical advice.

The authors deny any conflicts of interest related to this study.

References

1. Van Assche N, Vercruyssen M, Coucke W, Teughels W, Jacobs R, Quirynen M. Accuracy of computer-aided implant placement. Clin Oral Implants Res 2012;23 Suppl 6:112-123.
2. Torres A, Shaheen E, Lambrechts P, Politis C, Jacobs R. Microguided Endodontics: a case report of a maxillary lateral incisor with pulp canal obliteration and apical periodontitis. Int Endod J 2019;52(4):540-549.
3. Byun C, Kim C, Cho S, Baek SH, Kim G, Kim SG, et al. Endodontic Treatment of an Anomalous Anterior Tooth with the Aid of a 3-dimensional Printed Physical Tooth Model. J Endod 2015;41(6):961-965.
4. EzEldeen M, Wyatt J, Al-Rimawi A, Coucke W, Shaheen E, Lambrichts I, et al. Use of CBCT Guidance for Tooth Autotransplantation in Children. J Dent Res 2019;98(4):406-413.
5. Cui Z, Li C, Wang W. ToothNet: Automatic Tooth Instance Segmentation and Identification From Cone Beam CT Images. In: 2019 IEEE/CVF Conference on Computer Vision and Pattern Recognition (CVPR). Long Beach, CA, USA: IEEE; 2019. p. 6361-6370.
6. Shaheen E, Khalil W, Ezeldeen M, Van de Casteele E, Sun Y, Politis C, et al. Accuracy of segmentation of tooth structures using 3 different CBCT machines. Oral Surg Oral Med Oral Pathol Oral Radiol 2017;123(1):123-128.
7. Ludlow JB, Davies-Ludlow LE, Brooks SL, Howerton WB. Dosimetry of 3 CBCT devices for oral and maxillofacial radiology: CB Mercuray, NewTom 3G and i-CAT. Dentomaxillofac Radiol 2006;35(4):219-226.
8. EzEldeen M, Stratis A, Coucke W, Codari M, Politis C, Jacobs R. As Low Dose as Sufficient Quality: Optimization of Cone-beam Computed Tomographic Scanning Protocol for Tooth Autotransplantation Planning and Follow-up in Children. J Endod 2017;43(2):210-217.
9. Jacobs R, Salmon B, Codari M, Hassan B, Bornstein MM. Cone beam computed tomography in implant dentistry: recommendations for clinical use. BMC Oral Health 2018;18(1):88.
10. EzEldeen M, Van Gorp G, Van Dessel J, Vandermeulen D, Jacobs R. 3-dimensional analysis of regenerative endodontic treatment outcome. J Endod 2015;41(3):317-324.
11. Nguyen KCT, Duong DQ, Almeida FT, Major PW, Kaipatur NR, Pham TT, et al. Alveolar Bone Segmentation in Intraoral Ultrasonographs with Machine Learning. J Dent Res 2020;99(9):1054-1061.
12. Saha S. A Comprehensive Guide to Convolutional Neural Networks — the ELI5 way. 2018.
13. Kyong Hwan J, McCann MT, Froustey E, Unser M. Deep Convolutional Neural Network for Inverse Problems in Imaging. IEEE Trans Image Process 2017;26(9):4509-4522.
14. Lakhani P, Gray DL, Pett CR, Nagy P, Shih G. Hello World Deep Learning in Medical Imaging. J Digit Imaging 2018;31(3):283-289.
15. Litjens G, Kooi T, Bejnordi BE, Setio AAA, Ciompi F, Ghafoorian M, et al. A survey on deep learning in medical image analysis. Med Image Anal 2017;42:60-88.
16. Chen Y, Du H, Yun Z, Yang S, Dai Z, Zhong L, et al. Automatic Segmentation of Individual Tooth in Dental CBCT Images From Tooth Surface Map by a Multi-Task FCN. IEEE Access 2020;8:97296-97309.
17. Lee S, Woo S, Yu J, Seo J, Lee J, Lee C. Automated CNN-Based Tooth Segmentation in Cone-Beam CT for Dental Implant Planning. IEEE Access 2020;8:50507-50518.

18. Schwendicke F, Samek W, Krois J. Artificial Intelligence in Dentistry: Chances and Challenges. J Dent Res 2020;99(7):769-774.
19. Toennies KD. Segmentation and Basic Techniques. In: Guide to Medical Image Analysis - Methods and Algorithms. 2 ed. London: Springer; 2017. p. 208-247.
20. Akhoondali H, Zoroofi RA, Shirani G. Rapid automatic segmentation and visualization of teeth in CT-scan data. J. Applied Sci. 2009;9(11):2031-2044.
21. Toennies KD. The Level Set Model. In: Guide to Medical Image Analysis - Methods and Algorithms. 2 ed. London: Springer; 2017. p. 311-360.
22. Barrett WA, Mortensen EN. Interactive live-wire boundary extraction. Med Image Anal 1997;1(4):331-341.
23. Heckel F, Konrad O, Karl Hahn H, Peitgen H-O. Interactive 3D medical image segmentation with energy-minimizing implicit functions. Computers & Graphics 2011;35(2):275-287.
24. Kirillov A, He K, Girshick R, Rother C, Dollar. Panoptic Feature Pyramid Networks. In: The IEEE Conference on Computer Vision and Pattern Recognition (CVPR). 2018.
25. Rahman MA, Wang Y. Optimizing Intersection-Over-Union in Deep Neural Networks for Image Segmentation. In: Advances in Visual Computing. Springer; 2016. p. 234-244.
26. Cop R. Automatic teeth thresholding in cone beam CT with convolutional neural networks and tooth segmentation with the watershed transform. The Netherlands: University of Groningen; 2018.
27. Shahbazian M, Jacobs R, Wyatt J, Willems G, Pattijn V, Dhoore E, et al. Accuracy and surgical feasibility of a CBCT-based stereolithographic surgical guide aiding autotransplantation of teeth: in vitro validation. J Oral Rehabil 2010;37(11):854-859.
28. Jacobs R. Dental cone beam CT and its justified use in oral health care. JBR-BTR 2011;94(5):254-265.
29. Bland JM, Altman DG. Statistical methods for assessing agreement between two methods of clinical measurement. The Lancet 1986;1:307-310.
30. LeCun Y, Boser B, Denker JS, Henderson D, Howard RE, Hubbard W, et al. Backpropagation Applied to Handwritten Zip Code Recognition. Neural Comput 1989;1(4):541-551.
31. Zeiler MD, Fergus R. Visualizing and Understanding Convolutional Networks. In; 2014: Springer International Publishing; 2014. p. 818-833.
32. Tan M, Le QV. EfficientNet: Rethinking Model Scaling for Convolutional Neural Networks. In: 36th International Conference on Machine Learning. Long Beach, California; 2019.
33. Pauwels R, Jacobs R, Singer SR, Mupparapu M. CBCT-based bone quality assessment: are Hounsfield units applicable? Dentomaxillofac Radiol 2015;44(1):20140238.
34. Meschi N, EzEldeen M, Torres Garcia AE, Jacobs R, Lambrechts P. A Retrospective Case Series in Regenerative Endodontics: Trend Analysis Based on Clinical Evaluation and 2- and 3-dimensional Radiology. J Endod 2018;44(10):1517-1525.
35. Austah O, Joon R, Fath WM, Chrepa V, Diogenes A, Ezeldeen M, et al. Comprehensive Characterization of 2 Immature Teeth Treated with Regenerative Endodontic Procedures. J Endod 2018;44(12):1802-1811.

Table 1: Mean IoU/DSC performance comparison depending on tooth part, condition and type for SA, F-AI and R-AI

Figure 1: Architecture of the Feature Pyramid Network used. (A) The encoder extracts the interesting features from the input image, (B) the decoder generates a dense segmentation mask of the input and (C) the semantic segmentation branch combines the feature maps from all the layers of the decoder into one single output. (D) shows the result of multiple segmentation predictions and interpolations.

Figure 2: Workflow of the segmentation methods used. (A) and (B) represent ROI selection and rotation. (C) (D) and (E) show seeds and contour placement according to the three segmentation methods relying on semi-automated user segmentation (SA), Fully Automated AI-driven Segmentation (F-AI) and Refined AI-driven Segmentation (R-AI). (F) (G) and (H) show a 3D representation of CSOs contours. (I) (J) and (K) illustrate segmentation results for each method. (L) and (M) represent an example of a surface deviation map of F-AI (L) and R-AI (M) compared with the clinical reference (SA).

Figure 3: (A) A plot comparison between segmented volumes in mm^3 for SA, F-AI and R-AI. (B and C) Bland-Altman plots between tooth segmented volumes for F-AI (B) and R-AI (C) versus the clinical reference (SA) (the difference between the measurements is plotted against their mean). (D) IoU score comparison between F-AI and R-AI for Full tooth, crown and root segmentation (represented as mean with SD). (E) Median surface deviation from the clinical reference of F-AI and R-AI. (F and G) Morphologic surface comparison analysis of SA versus F-AI (F) and R-AI (G).

Table 1: Mean IoU/DSC performance comparison depending on tooth part, condition and type for SA, F-AI and R-AI

	SA vs F-AI Full tooth	**SA vs R-AI Full tooth**	**SA vs F-AI Crown**	**SA vs R-AI Crown**	**SA vs F-AI Root**	**SA vs R-AI Root**	**SA vs F-AI Mature teeth**	**SA vs R-AI Mature teeth**
IoU	0.877 (±0.037)	0.881 (±0.036)	0.887 (±0.032)	0.889 (±0.036)	0.894 (±0.03)	0.898 (±0.026)	0.876 (±0.039)	0.881 (±0.038)
DSC	0.934 (±0.02)	0.937 (±0.02)	0.940 (±0.018)	0.941 (±0.02)	0.944 (±0.017)	0.946 (±0.014)	0.934 (±0.023)	0.937 (±0.021)
	SA vs F-AI Immature teeth	**SA vs R-AI Immature teeth**	**SA vs F-AI Incisors**	**SA vs R-AI Incisors**	**SA vs F-AI Canines**	**SA vs R-AI Canines**	**SA vs F-AI Premolars**	**SA vs R-AI Premolars**
IoU	0.879 (±0.032)	0.884 (±0.031)	0.877 (±0.038)	0.881 (±0.035)	0.898 (±0.027)	0.906 (±0.029)	0.891 (±0.025)	0.890 (±0.022)
DSC	0.935 (±0.018)	0.938 (±0.018)	0.934 (±0.024)	0.937 (±0.022)	0.949 (±0.012)	0.954 (±0.013)	0.942 (±0.011)	0.94 (±0.0078)

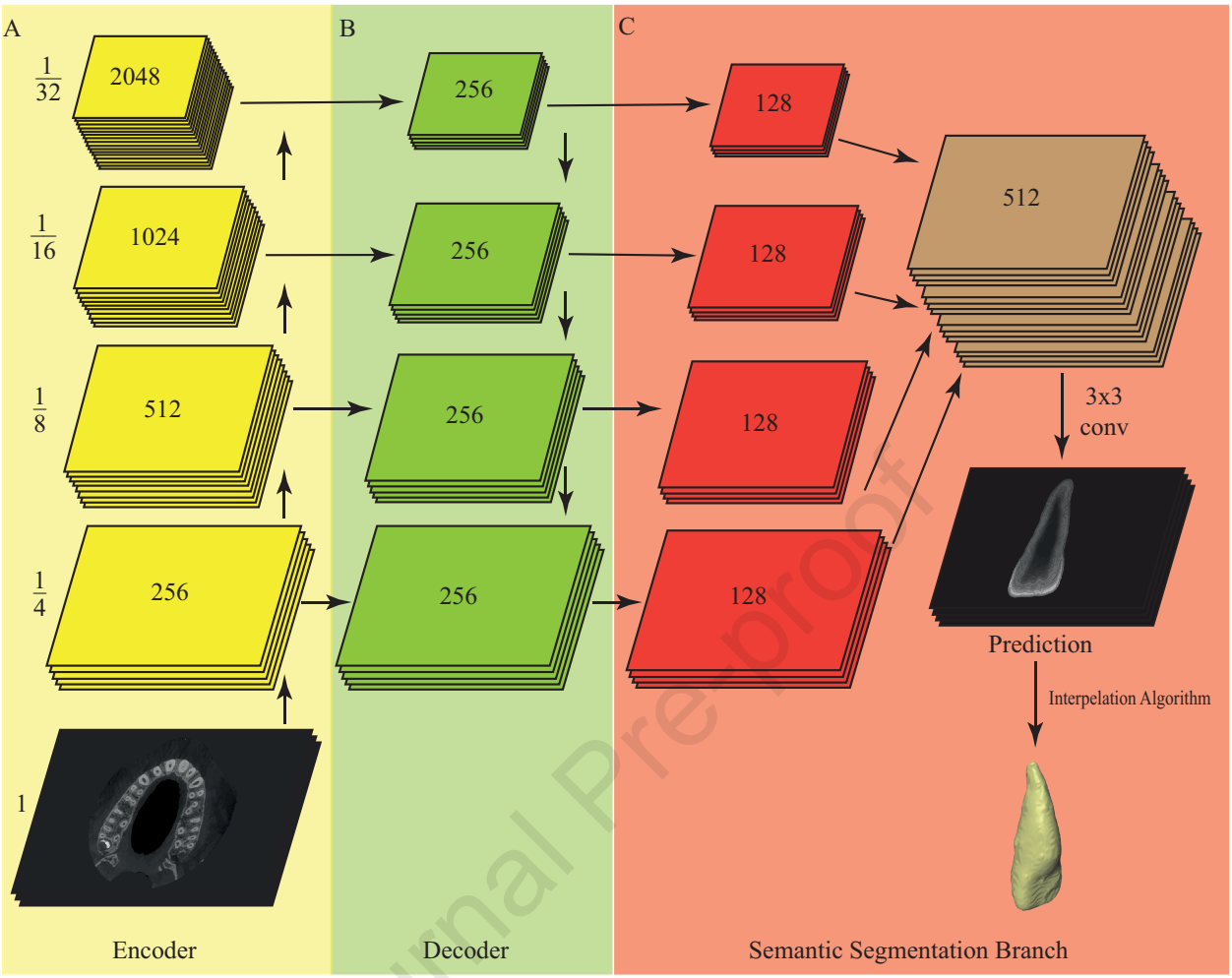

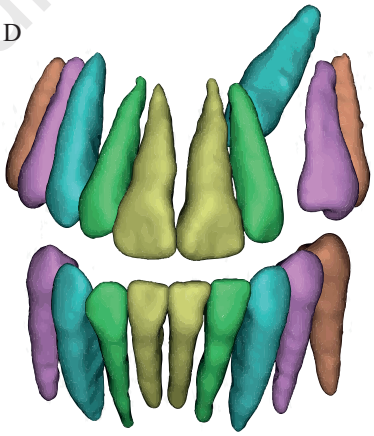

Multiple Segmentation Prediction and Interpolation

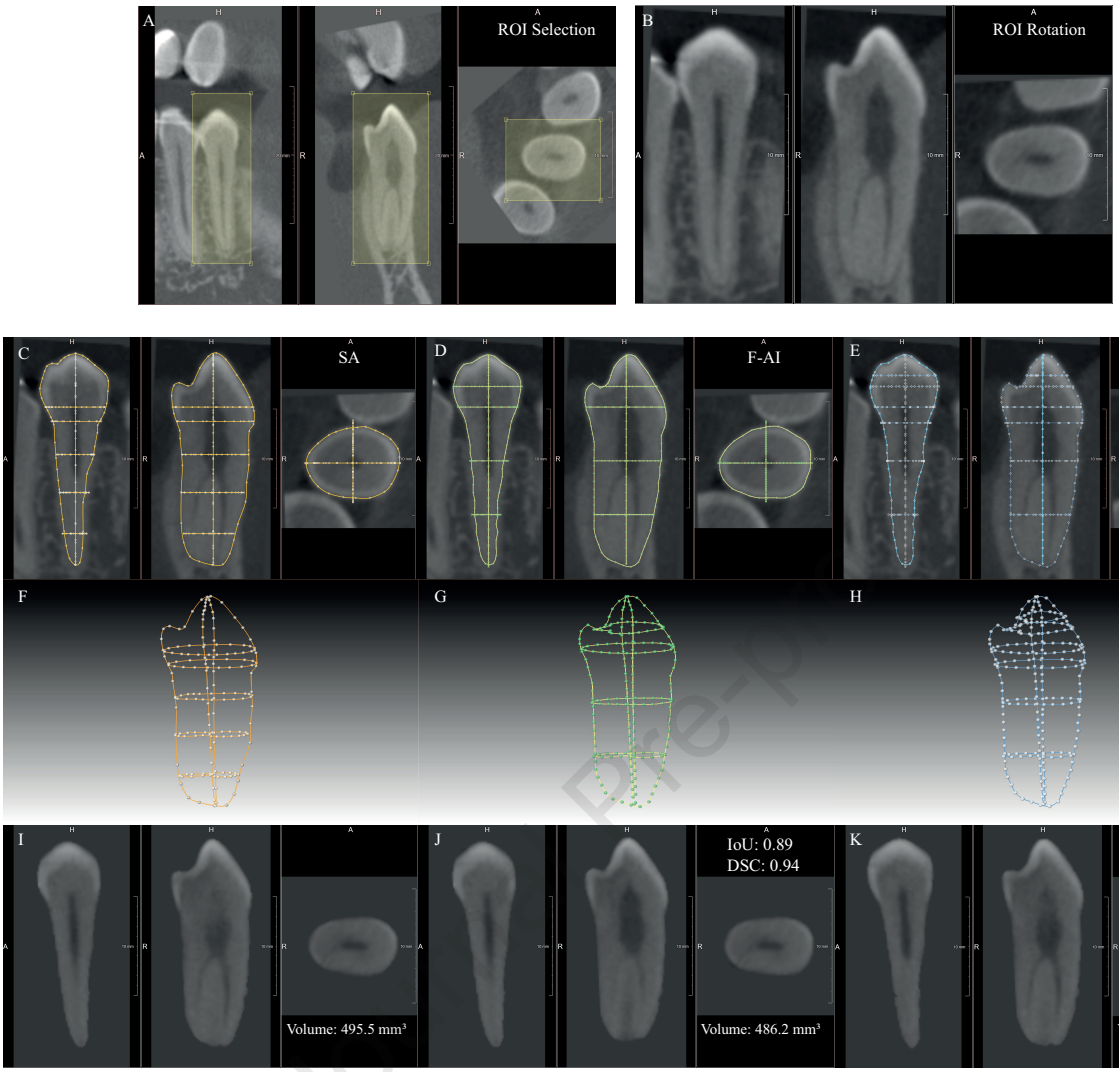
A
ROI Selection
B
ROI Rotation
C
SA
D
F-AI
E
R-AI
F
G
H
I
Volume: 495.5 mm³
J
IoU: 0.89
DSC: 0.94
Volume: 486.2 mm³
K
IoU: 0.90
DSC: 0.95
Volume: 489.1 mm³

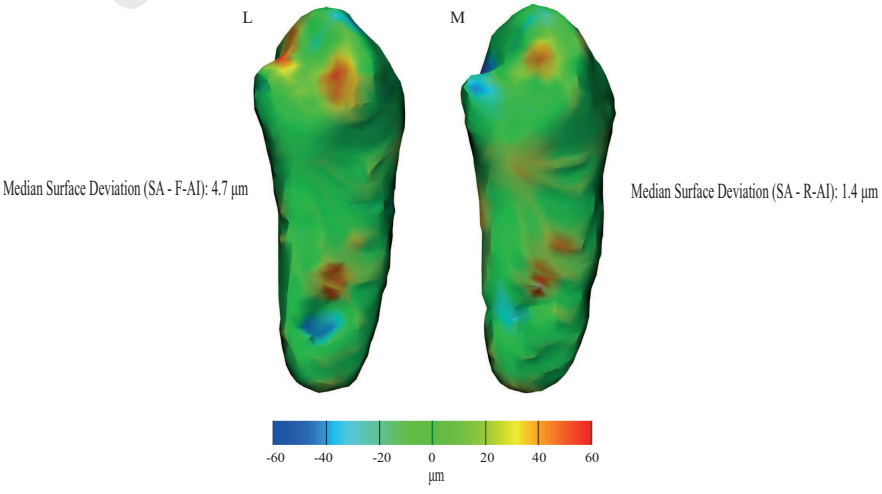
L
M
Median Surface Deviation (SA - F-AI): 4.7 µm
Median Surface Deviation (SA - R-AI): 1.4 µm
-60
-40
-20
0
20
40
60
µm